ACS APPLIED MATERIALS & INTERFACES

Research Article

www.acsami.org

Bottom-up Growth of Hierarchical Electrodes for Highly Efficient Dye-Sensitized Solar Cells

Youngshin Lee, Chang-Yeol Cho, Su-Jin Ha, Hye-Na Kim, and Jun Hyuk Moon*

Department of Chemical and Biomolecular Engineering, Sogang University, Seoul 121-742, South Korea

Supporting Information

ABSTRACT: The nonconventional bottom-up growth of TiO_2 was first demonstrated in the preparation of hierarchical TiO_2 electrodes for use in highly efficient dye-sensitized solar cells. The simple immersion of a substrate in a precursor solution enabled the growth of TiO_2 particulate films. Here, we have implemented a hierarchical growth strategy in which two stages of controlled growth yielded first macroscale TiO_2 particles, followed by mesoscale TiO_2 particles. We successfully fabricated electrode films up to 20 μm thick via a growth rate of 0.3 μm/min. The specific area of the electrodes was controlled via the deposition of mesoscale TiO_2 particles. The deposited particles displayed a rutile phase with an average size of several tens of nanometers in diameter, as confirmed by XRD and high-resolution TEM imaging. After depositing the second layer of mesoscale TiO_2 particles, the photocurrent density increased by a factor of 3. A maximum efficiency of 6.84% was obtained for the hierarchically structured TiO_2 electrodes under 1 sun illumination. The hierarchical TiO_2 electrodes were compared with macroporous TiO_2 electrodes, revealing that the higher photocurrent density could be attributed to a longer electron recombination lifetime and a high specific area. The longer recombination lifetime was supported by the presence of fewer defective TiO_2 surfaces, as confirmed by the XPS spectrum.

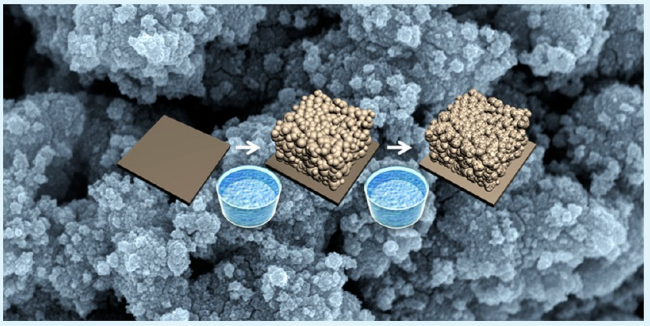

KEYWORDS: *hierarchical structures, solution deposition, TiO_2, macroporous, recombination lifetime, dye-sensitized solar cells*

INTRODUCTION

Dye-sensitized solar cells (DSSCs) based on oxide semiconductors and organic dyes or metallo-organic complex dyes have attracted much attention because of their low production costs and their unique advantages for fabricating transparent cells over silicon or thin-film solar cells.[1] DSSCs employ a wide band gap semiconductor, such as a TiO_2 nanoparticle film, to provide a mesoporous structure with a large specific area for the adsorption of light-harvesting dye molecules.[2] Although recent work by Grätzel et al. updated the record of photon-to-electric conversion efficiency to 12%,[3] an efficiency ceiling of 11% has persisted for nearly two decades. The limit in efficiency has been mainly attributed to the recombination of the photogenerated electrons during electron transport through the nanoparticulate electrode.[4] To address these issues, several efforts have focused on engineering microstructured electrodes.

Electrode engineering was initially achieved by utilizing directional and/or ordered macroscale (>50 nm) morphologies, such as nanotubes,[5,6] nanowires,[7] or 3D periodic inverse opals.[8] Many promising results have reported increases in electron transport by up to 4 times or in electron lifetimes by 2−4 times,[9,10] but the external conversion efficiencies have remained at 70−80% of the efficiency record. One issue is that the specific areas of these macroscale morphologies are low; therefore, they yield a low absorption of dye molecules and thereby low photocurrent density under illumination. For example, cells comprising nanotube array electrodes yield 70% of the dye adsorption and 50% of the short-circuit current density of conventional nanoparticle electrodes, resulting in a 30−50% lower conversion efficiency.[11−13] This limitation has led the utilization of hierarchical structures that combine macro and mesoscale morphologies. Macroscale morphologies enhance light absorption efficiency, electron transport, and facilitate infiltration of polymeric electrolytes. Mesoscale morphologies allow high specific areas for dye adsorption. Previously, the hierarchical structures have been fabricated using a simple strategy of sequential growth of mesoscale morphologies on macroscale structure, for example, nanoparticles decoration on nanotubes, nanowires, or 3D inverse opal structures.[14−18] An additional layer of macroscale structures, such as nanotubes or inverse opals has been introduced on top of a conventional mesoporous electrode.[19,20] Occasionally, a growth in heated pressurized solution or physical deposition in vacuum has been employed to directly grow the hierarchical structures.[21−23]

In this paper, we demonstrated a facile approach to preparing hierarchically structured electrodes via nonconventional, bottom-up growth approach. Briefly, the deposition of TiO_2

Received: April 15, 2012
Accepted: June 14, 2012
Published: June 27, 2012

   dx.doi.org/10.1021/am300664x | ACS Appl. Mater. Interfaces 2012, 4, 3589−3595

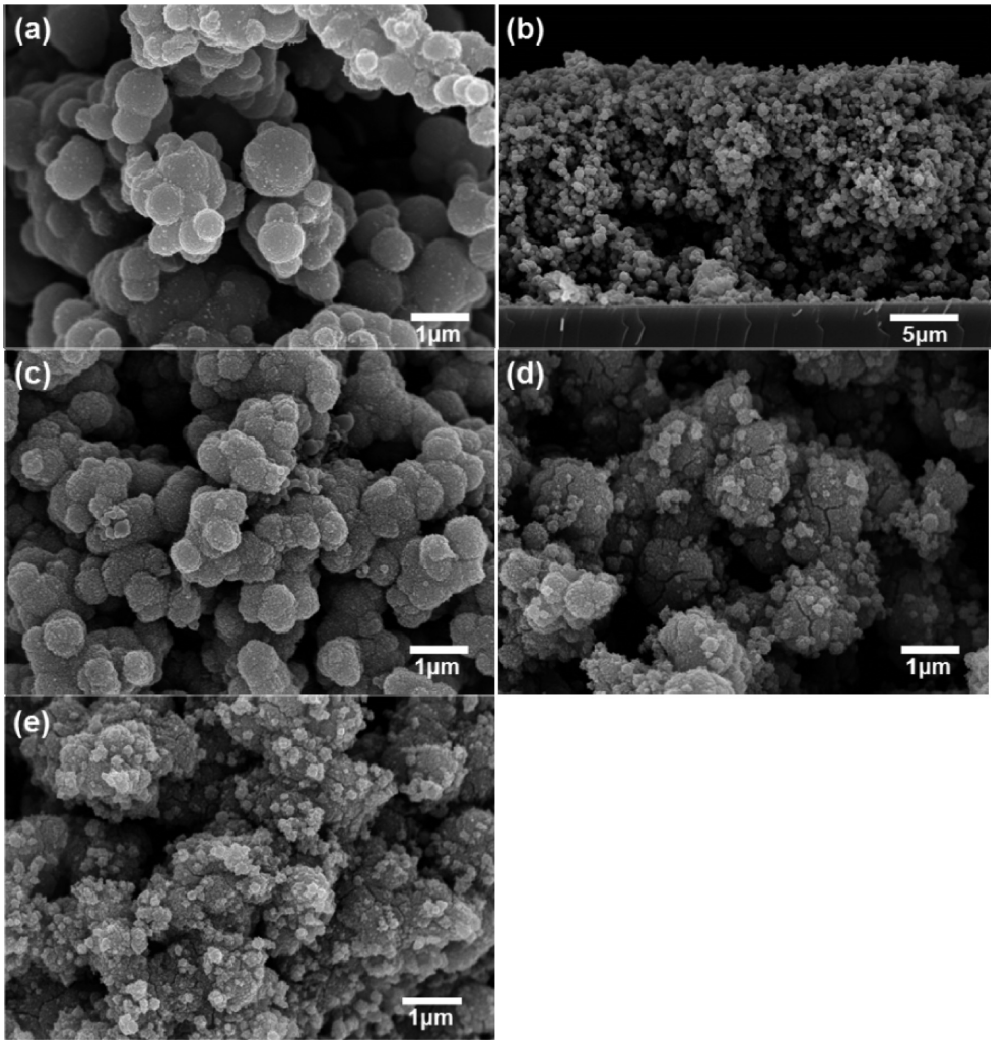

Figure 1. (a, b) SEM images of particulate TiO_2 films on an FTO substrate after the first growth stage; the film cross-section is also shown. (c–e) SEM images of a TiO_2 particulate film after the second stage of deposition, with growth periods of 30, 60, and 90 min.

particles on a substrate was achieved by dipping the substrate into a chemical bath of the precursor solution. Multiple coating stages produced hierarchical meso–macroscale particulate electrodes. The first deposition stage produced micrometer to submicrometer particulate films, and subsequent deposition produced mesoscale particles on the surfaces of the deposited films. Using this approach, we avoided multiple steps for the preparation of TiO_2 nanoparticle suspension and careful control of the suspension properties and adhesion, which is generally required to form conventional electrodes. Moreover, the deposition achieved in solution at atmospheric pressure may be more high-throughput compared to the aforementioned physical deposition and hydrothermal growth approaches. Briefly, the growth rate during the first deposition stage was controlled via the precursor concentration and the solution bath temperature. Specifically, the subsequent second deposition stage permitted control over the specific area of the electrodes by depositing mesoscale TiO_2 particles. We evaluated the effects of second deposition time on the photovoltaic properties and the efficiency of DSSCs. The maximum photon-to-electric conversion efficiency achieved using our hierarchical TiO_2 electrodes was 6.84%.

EXPERIMENTAL SECTION

Preparation of the Hierarchical TiO_2 Films. A fluorine-doped SnO_2 (FTO, 8 Ohm/square) transparent conducting glass substrate was used as an electrode substrate. The transparent conducting substrate was used as a substrate for fabricating TiO_2 electrodes. A seed layer for the bottom-up growth of TiO_2 was prepared by spin-coating a 0.9 M $TiCl_4$ ethanol solution onto the FTO substrate, followed by heating to 450 °C for 30 min. The film was then exposed to UV light (Oriel, 150 W xenon arc lamp) for 5 min to activate the TiO_2 seed layer. The first TiO_2 layer growth stage proceeded by immersion the seed layer-coated FTO substrate glass in the $TiCl_4$ aqueous solution bath. Typically, a 0.5 M $TiCl_4$ aqueous solution prepared at 0 °C in an ice water bath with vigorous stirring was heated to 80 °C. This bath was used to grow the first layer of TiO_2. The deposition time was around 1 h for the growth of a 20 μm thick film. After growth, the TiO_2 film was heated to 500 °C for 15 min. Mesoscale TiO_2 particles were then deposited onto the first layer by immersing the first TiO_2 layer on the FTO substrate into the $TiCl_4$ aqueous solution. A 0.3 M $TiCl_4$ solution and a 70 °C bath temperature were used.

Fabrication of DSSCs Using the Hierarchical TiO_2 Electrodes. A hierarchical film was scraped to obtain a 5 mm × 5 mm active area. The bottom-up grown TiO_2 film was immersed in a dye solution for 20 h to yield a sensitized electrode. The dye solution was prepared by dissolving N719 (Dyesol) in 2-propyl alcohol (anhydrous, Aldrich). The counter electrode was prepared by coating a 0.5 mM H_2PtCl_6

solution in anhydrous ethanol onto an FTO substrate, followed by sintering at 450 °C for 30 min. The TiO_2 electrode and Pt counter electrode were assembled and sealed to a thickness of 60 μm using Surlyn (Dupont) spacers. The electrolyte (Iodolyate An-50, Solaronix) was injected into the gap.

Photovoltaic Measurements. The simulated solar light was achieved using a xenon lamp (300 W, Oriel) and an AM1.5 filter. The incident light intensity was calibrated using a standard Si solar cell. The I–V curves were obtained by measuring the photocurrent using a source meter (Keithley, model 2400). The incident photon-to-electric conversion efficiency (IPCE) measurements were obtained using a source meter under monochromatic light. Electrochemical impedance spectroscopy (EIS) was performed using an impedance analyzer (Versastat, AMETEK). The impedance spectra were measured under 100 mW/cm^2 illumination under open circuit conditions. The frequency range explored in the impedance measurements was 1×10^5 Hz to 0.1 Hz.

Characterizations. TiO_2 electrode surfaces were imaged by scanning electron microscopy (FE-SEM, Hitachi S4700) operated at an accelerating voltage of 15 kV. A high-resolution image of the deposited TiO_2 particles was observed by transmission electron microscopy (TEM, Hitachi H8100). The crystalline phase of the TiO_2 films was analyzed by X-ray diffraction (XRD, Rigaku) techniques, and the chemical components of the TiO_2 surface were analyzed by X-ray photoelectron spectroscopy (XPS, ESCALAB 250 XPS System, Thermo Fisher Scientific) using monochromated Al Kα X-ray source at 1486.6 eV. The amount of dye molecules adsorbed onto the TiO_2 electrodes was quantified by measuring the absorption of N719 molecules detached from sensitized TiO_2 surfaces via UV–vis spectrophotometry (JASCO V550).

RESULTS AND DISCUSSION

The bottom-up growth of hierarchical TiO_2 electrodes is briefly described. First, the formation of a TiO_2 seed layer was required to grow TiO_2 particles on a fluorine-doped SnO_2 (FTO) glass substrate. The first growth stage in an aqueous TiO_2 precursor solution yielded a macroscale TiO_2 layer consisting of particles with submicrometer diameters. This layer provided a scaffold TiO_2 structure for the second deposition. The second growth stage was achieved using the same type of precursor solution bath, this time depositing mesoscale TiO_2 particles 10–100 nm in diameter.

Here, the growth of the TiO_2 film on the FTO substrate or on a layer of deposited TiO_2 was achieved using a sol–gel reaction of $TiCl_4$.[24,25] The growth rate of the particulate film, and the size and shape of the primary TiO_2 particles were governed by the concentration, pH and temperature of the $TiCl_4$ precursor solution. Briefly, a higher growth rate and larger TiO_2 particles were obtained at higher precursor solution temperatures and concentrations. During the first growth stage, the temperature was set to 80 °C and a 0.5 M $TiCl_4$ solution was used to obtain, on average, a 0.3 μm/min rate of deposition to yield a 20 μm thick film. At low bath temperatures, below 70 °C, and using 0.3 M $TiCl_4$ aqueous solutions, the reaction was too slow to obtain useful coatings within a few hours. The TiO_2 particle diameter was below 100 nm. Above 90 °C, the growth rate was too high to achieve reproducible film thicknesses and the TiO_2 particle size was above 1 μm in diameter. Within the range 70–80 °C and for a 0.5 M $TiCl_4$ bath, the average growth rate was 0.2–0.3 μm/min, and the average TiO_2 particle diameter was 200–800 nm. At 80 °C and a 0.5 M $TiCl_4$ solution, loosely packed TiO_2 particles 500–800 nm in diameter were obtained, as shown in a and b in Figure 1. Figure 1b also shows a cross-section of the first stage growth layer 20 μm thick.

The second deposition layer was introduced over the first layer after heat treatment of the film to allow for the complete condensation of TiO_2 particles. It should be noted that the initial deposition of TiO_2 particles (even under identical conditions) was slow because of the tremendous increase in the TiO_2 surface area after the first growth stage. This surface area provided additional nucleation sites for the second deposition stage. The range of precursor solution conditions mentioned above, along with a 2 h growth period, yielded a high number of nucleation sites that facilitated the growth of TiO_2 particles 10–100 nm in diameter. Here, during the second deposition stage, the deposition time was increased from 0 to 30 min, 60 min, and 90 min. The corresponding number of mesoscale TiO_2 particles deposited on the first layer increased, as shown in Figure 1c–e. The specific surface area of the particulate TiO_2 films was quantified by measuring the dye adsorption, as shown in Table 1. Compared to the dye adsorption levels achieved by

Table 1. Summary of the Measured Photovoltaic Parameters J_{SC}, V_{OC}, FF, Calculated Photon-to-Electric Conversion Efficiency (Eff) of DSSCs Prepared Using TiO_2 Photoelectrodes Produced with Various Second Deposition Stage Growth Times, and Amounts of Adsorbed Dye

second deposition stage growth time (min)	J_{SC} (mA/cm^2)	V_{OC}(V)	FF (%)	Eff (%)	amount of adsorbed dye (mmol/cm^2)
0 (ref)	9.62	0.68	60	3.96	0.021
30	9.66	0.71	58	3.95	0.022
60	15.43	0.68	58	6.10	0.050
90	17.67	0.68	57	6.84	0.053

the first stage of TiO_2 layer growth, the second stage of growth produced dye adsorption levels that were 2.5 and 2.8 times higher with second stage deposition times of 60 and 90 min, respectively. Meanwhile, the deposited TiO_2 layer showed a relatively strong adhesion to the substrate under the Scotch tape test (see Figure S1 in the Supporting Information).

TiO_2 particles grown during the first growth stage or during the second deposition stage were further investigated by TEM, as shown in images a and b and images c and d in Figure 2, respectively. The TiO_2 particles produced by the first growth stage formed via the aggregation of elliptical particles 50 nm in length and 25 nm in width. The high-resolution image shown in Figure 2b reveals the atomic lattice of the TiO_2; the distance between fringes was 0.33 and 0.17 nm, which corresponded to the *d*-spacings of the (110) and (211) planes of rutile TiO_2.[26] After the second deposition stage, the films clearly revealed particles with rougher surfaces than were observed after the first growth stage. Particles were covered by rod-like particles around 25 nm long. The high-resolution images showed atomic lattices of 0.33 and 0.21 nm, corresponding to *d*-spacings of the (111) and (211) planes of rutile TiO_2.[26] Meanwhile, X-ray diffraction (XRD) patterns of the TiO_2 films after the first growth stage and after the subsequent deposition stage are shown in Figure S2 in the Supporting Information. Previously, the crystal phase of TiO_2 was determined by the pH of the precursor solution, presence of salt, as well as the reaction condition.[27–29] The synthesis of TiO_2 via a sol–gel reaction of the aqueous $TiCl_4$ precursor favored the rutile phase of TiO_2 due to the acid environment, whereas the solution with the addition of basic additive produced more anatase phase.[28] Here, the intensity of the rutile peak increased over time during the second deposition stage, whereas the anatase peak intensity

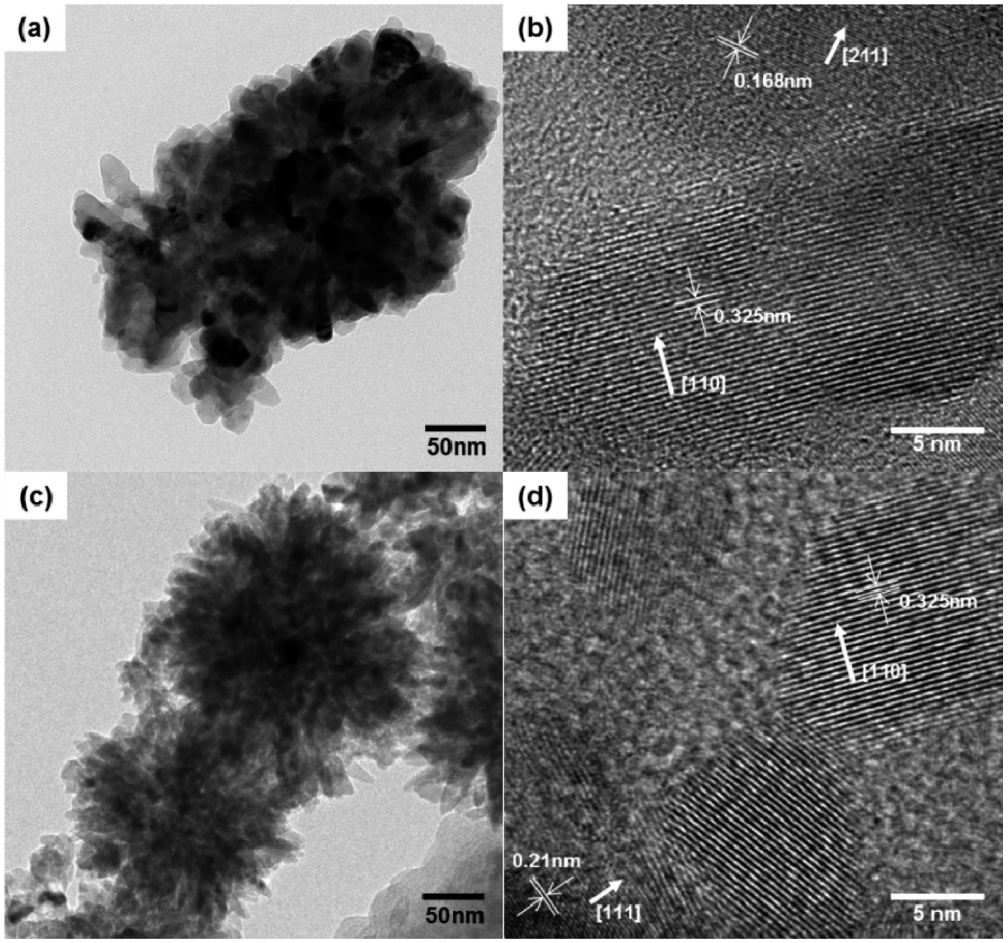

Figure 2. (a, b) TEM images of TiO_2 particles produced by the first growth stage, and (c, d) TEM images of TiO_2 particles produced after the second deposition stage, with a growth period of 90 min. The arrows in b and d indicate the direction perpendicular to the lattice plane.

remained constant. This indicated that the rutile TiO_2 mesoscale particles grew over a first layer of TiO_2 particles. The TEM images shown in Figure 3a,c clearly revealed the growth of rodlike rutile TiO_2 particles, which densely coated the first layer of deposited TiO_2 particles.

The chemical state of the TiO_2 surfaces after the first growth stage and the second deposition stage were investigated by X-ray photoelectron spectroscopy (XPS). The oxidation state or the concentration of oxygen vacancies in a TiO_2 surface is related to the electron transport/recombination in addition to the efficiency of dye adsorption.[30,31] Figure 4 shows the Ti 2p photoelectron spectra of a TiO_2 film after the first growth stage and after the subsequent deposition stage of TiO_2 particles. The four peaks of Ti^{4+} $2p_{1/2}$, Ti^{3+} $2p_{1/2}$, Ti^{4+} $2p_{3/2}$, and Ti^{3+} $2p_{3/2}$ were used to deconvoluted the spectra.[32] The main peaks at 458.5 and 464.0 eV were attributed to Ti^{4+} or TiO_2, and the peaks at 457.0 and 462.8 eV corresponded to Ti^{3+} surface states, i.e., oxygen vacancies. The XPS spectra obtained after the first or second growth stages differed significantly in that the TiO_2 surface after the first growth stage presented Ti^{3+}, and this peak intensity was reduced after the second deposition stage. This may be explained in terms of the growth rates during the first and second deposition stages. As mentioned, the growth rate during the first growth stage was fast, and the resultant TiO_2 particles were more likely to include defects in the crystal lattice than were particles produced during the much slower second deposition stage. TiO_2 surfaces with fewer oxygen vacancies yield higher dye molecule adsorption densities. TiO_2 surfaces with fewer defects also promote electron transport

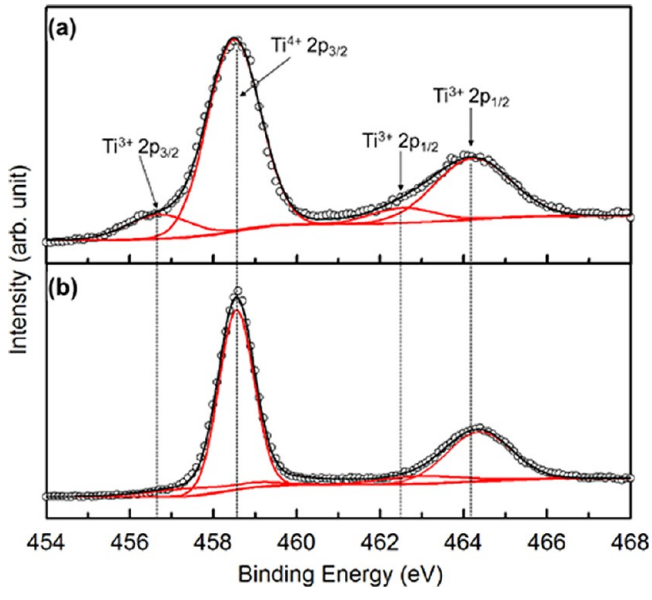

Figure 3. XPS Ti2p spectrum of the TiO_2 film (a) without and (b) with the second deposition stage with a growth rate of 90 min; experimental data (circle), four deconvoluted spectra (red solid line), summation of the four spectra (black solid line).

dx.doi.org/10.1021/am300664x | ACS Appl. Mater. Interfaces 2012, 4, 3589−3595

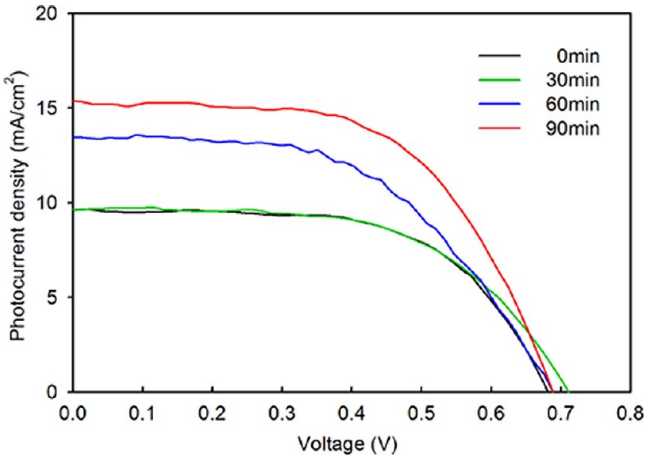

Figure 4. Photocurrent density–voltage (I–V) curves of DSSCs prepared using a TiO_2 electrode produced by the first growth stage, or a hierarchical TiO_2 electrode prepared using an electrode produced with various second deposition stage growth times.

because oxygen vacancy hinder electron transport in TiO_2 films by trapping and detrapping electrons, as further discussed below.

Hierarchical TiO_2 films 20 μm thick were fabricated via a first growth stage and a subsequent second deposition stage, and were then used as photoelectrodes in DSSCs. We investigated the effects of the mesoscale TiO_2 particle coating density on the photovoltaic performance. The curves in Figure 4a show the current–voltage (I–V) characteristics of the DSSCs containing the hierarchical electrodes, for various second deposition times and Table 1 lists their photovoltaic parameters; the short-circuit photocurrent density (J_{SC}), open-circuit voltage (V_{OC}), and fill factor (FF) are reported for each film. The overall conversion efficiency (Eff) of each cell was calculated according to the equation, Eff = $J_{SC}V_{OC}$FF/P, where P is the incident light intensity, 100 mW/cm^2. J_{SC} was found to increase significantly from 9.6 mA/cm^2 to 17.7 mA/cm^2 as the second deposition growth time was increased to 90 min. The corresponding efficiencies increased from 4.0 to 6.7%. Figure S3 in the Supporting Information shows the incident photon-to-current efficiency (IPCE) spectra of the hierarchical electrodes prepared with a hierarchical electrode (90 min deposition time) and a reference TiO_2 electrode. The hierarchical electrode yielded a 56% peak IPCE, whereas the reference electrode yielded only a 20% peak IPCE. Thus, the IPCE spectra confirmed that the second deposition stage enhanced the J_{SC}. Compared with the conventional nanocrystalline TiO_2 electrodes with similar thickness,[33] our TiO_2 electrodes showed a relatively low FF. This result might be due to lower contact area of the hierarchical electrodes with the substrate, resulting in higher contact resistance, or slower electron diffusion in rutile TiO_2 electrodes.[34]

The enhancement in J_{SC} was mainly attributed to the increase in the specific area, which permitted more dye adsorption and, therefore, a higher light harvesting efficiency. The SEM and TEM images clearly displayed rougher surfaces after the second deposition stage and for longer growth times. Quantitative analysis of the specific areas of the TiO_2 surfaces via dye adsorption measurements also confirmed that the adsorption density after a 90 min deposition time was 2.5 times the absorption density of the reference electrode. Electrochemical impedance spectroscopy (EIS) was used to characterize electron transport in the hierarchical electrodes by comparison with the reference electrode, as shown in Figure 5.[35,36] The Nyquist plot in Figure 5a revealed a large semicircle

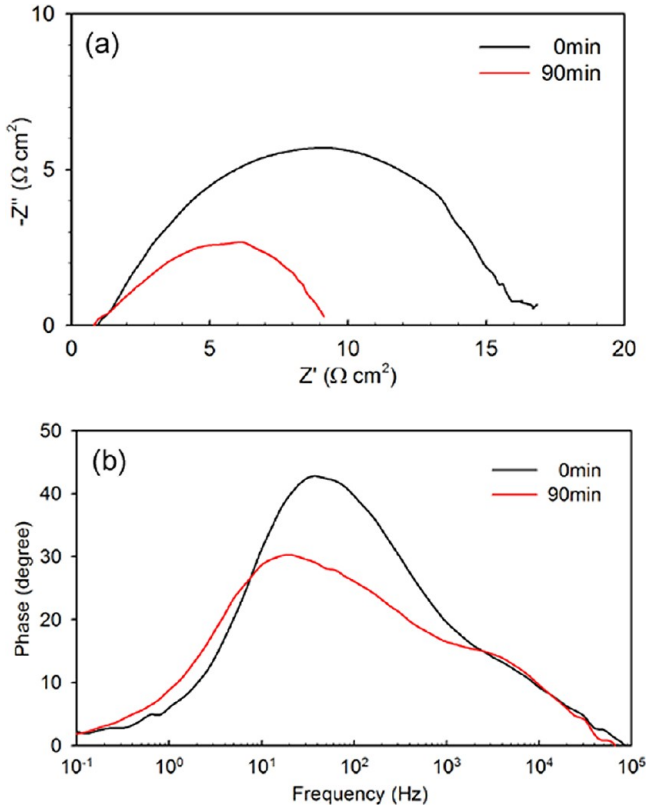

Figure 5. Impedance spectra of DSSCs comprising TiO_2 electrodes without and with a 90 min second deposition stage, measured under 1 sun illumination at an open circuit potential. (a) Nyquist plots, (b) Bode phase plots.

in the frequency range between 1 kHz and 100 Hz. The size of the arc depends on the concentration of I^{3-} and the rate of back-electron transfer at the TiO_2/electrolyte interface. The impedance spectrum was analyzed using an equivalent circuit for the TiO_2/electrolyte interface in the conductive state. The chemical capacitance (C_μ) and charge-transfer resistance or recombination resistance (R_r) were obtained by fitting the curve of the large semicircle. The values of R_r for the hierarchical TiO_2 electrode and reference sample were estimated to be 8 Ω cm^2 and 15 Ω cm^2, respectively. The decrease in R_r, which corresponded to a higher rate of electron recombination, could be explained in terms of the higher specific area of the hierarchical TiO_2 electrodes, which increased the number of traps, slowed down electron transport, and increased the recombination rate. The value of C_μ for the hierarchical TiO_2 electrodes was around three times the value of the reference sample because the dye adsorption density and, therefore, the electron injection density, were higher. The combination of R_r and C_μ determines the characteristic time scale for electron recombination. The recombination lifetimes were higher for the hierarchical TiO_2 electrodes by a factor of 2. The increase in the electron lifetime was confirmed using Bode phase plots, as shown in Figure 5b. The electron lifetime could be calculated based on the inverse of the peak frequency of the plot.[35,36] The peak frequency of the hierarchical electrode (20 Hz) was half the value of the reference sample (40 Hz), which

dx.doi.org/10.1021/am300664x | ACS Appl. Mater. Interfaces 2012, 4, 3589–3595

confirmed the above analysis. As the specific area of the TiO_2 electrodes increased during the second deposition stage, the larger increase in C_μ, compared to the smaller decrease in R_t, extended the electron lifetime in the hierarchical electrode and indicated different trap densities in the TiO_2 surfaces. In other words, a less defective TiO_2 surface in the hierarchical electrodes, consistent with the XPS analysis, may have increased the electron lifetimes.

CONCLUSION

This work demonstrated the nonconventional fabrication of hierarchically structured TiO_2 electrodes for use in DSSCs, based on a bottom-up growth strategy. Here, a two-step growth strategy was applied: the first growth stage deposited macroporous TiO_2 films. The average growth rate was controlled by the concentration and temperature of the solution bath, and was as high as 0.3 μm/min. The second growth stage deposited mesoscale TiO_2 particles several tens of nanometers in length on the surface of the first layer. The deposition of mesoscale particles was controlled by the immersion time in a precursor solution bath. As the immersion time increased from 0 min (first growth stage only) to 90 min, the specific area, measured according to the dye adsorption density, increased by a factor of 3. Moreover, compared to the TiO_2 surface produced from the first growth, the surface produced by the second deposition stage provided fewer oxygen vacancies in the TiO_2 crystals, as confirmed by the XPS spectrum. The photovoltaic performances of cells were evaluated as a function of the deposition time used to prepare the mesoscale TiO_2 particles. As the mesoscale TiO_2 particle deposition time increased, the J_{SC} increased significantly by up to a factor of 1.5. The maximum efficiency was 6.84% for hierarchical TiO_2 electrodes prepared with a 90 min second deposition growth time. The higher photocurrent density was attributed to a higher specific area in the hierarchical TiO_2 electrodes. The EIS measurements yielded higher electron lifetimes in the hierarchical TiO_2 electrodes. The bottom-up growth strategy provided a simple high-throughput approach to fabricating particulate TiO_2 electrodes and hierarchically structured electrodes. Our group is extending this work to studies of the deposition of a variety of oxide layers or particles, such as ZnO and Nb_2O_5, which could further enhance the photon conversion efficiency, potentially approaching the conversion efficiencies of conventional nanocrystalline TiO_2 electrodes.

ASSOCIATED CONTENT

Supporting Information

Adhesion test, XRD patterns, and IPCE spectrum. This material is available free of charge via the Internet at http://pubs.acs.org.

AUTHOR INFORMATION

Corresponding Author

*E-mail: junhyuk@sogang.ac.kr.

Notes

The authors declare no competing financial interest.

ACKNOWLEDGMENTS

This work was supported by the Seoul R&BD Program (ST100057). The Korea Basic Science Institute is also acknowledged for SEM, TEM, and XPS measurements.

REFERENCES

(1) Oregan, B.; Grätzel, M. *Nature* **1991**, *353*, 737−740.
(2) Papageorgiou, N.; Barbe, C.; Grätzel, M. *J. Phys. Chem. B* **1998**, *102*, 4156−4164.
(3) Yella, A.; Lee, H. W.; Tsao, H. N.; Yi, C. Y.; Chandiran, A. K.; Nazeeruddin, M. K.; Diau, E. W. G.; Yeh, C. Y.; Zakeeruddin, S. M.; Grätzel, M. *Science* **2011**, *334*, 629−634.
(4) Hagfeldt, A.; Boschloo, G.; Sun, L. C.; Kloo, L.; Pettersson, H. *Chem. Rev.* **2010**, *110*, 6595−6663.
(5) Kim, D.; Ghicov, A.; Albu, S. P.; Schmuki, P. *J. Am. Chem. Soc.* **2008**, *130*, 16454−16455.
(6) Prakasam, H. E.; Shankar, K.; Paulose, M.; Varghese, O. K.; Grimes, C. A. *J. Phys. Chem. C* **2007**, *111*, 7235−7241.
(7) Law, M.; Greene, L. E.; Johnson, J. C.; Saykally, R.; Yang, P. D. *Nat. Mater.* **2005**, *4*, 455−459.
(8) Shin, J. H.; Moon, J. H. *Langmuir* **2011**, *27*, 6311−6315.
(9) Ohsaki, Y.; Masaki, N.; Kitamura, T.; Wada, Y.; Okamoto, T.; Sekino, T.; Niihara, K.; Yanagida, S. *Phys. Chem. Chem. Phys.* **2005**, *7*, 4157−4163.
(10) Mor, G. K.; Shankar, K.; Paulose, M.; Varghese, O. K.; Grimes, C. A. *Nano Lett.* **2006**, *6*, 215−218.
(11) Jennings, J. R.; Ghicov, A.; Peter, L. M.; Schmuki, P.; Walker, A. B. *J. Am. Chem. Soc.* **2008**, *130*, 13364−13372.
(12) Varghese, O. K.; Paulose, M.; Grimes, C. A. *Nat. Nanotechnol.* **2009**, *4*, 592−597.
(13) Koo, H. J.; Kim, Y. J.; Lee, Y. H.; Lee, W. I.; Kim, K.; Park, N. G. *Adv. Mater.* **2008**, *20*, 195−199.
(14) Cao, G. Z.; Chou, T. P.; Zhang, Q. F.; Fryxell, G. E. *Adv. Mater.* **2007**, *19*, 2588−2592.
(15) Tan, B.; Wu, Y. Y. *J. Phys. Chem. B* **2006**, *110*, 15932−15938.
(16) Wang, X. D.; Qiu, J. H.; Guo, M. *ACS Appl. Mater. Interfaces* **2011**, *3*, 2358−2367.
(17) Cho, C. Y.; Moon, J. H. *Adv. Mater.* **2011**, *23*, 2971−2975.
(18) Qiu, J. J.; Zhuge, F. W.; Li, X. M.; Gao, X. D.; Gan, X. Y.; Yu, W. D. *Adv. Mater.* **2011**, *23*, 1330−1334.
(19) Zheng, Q.; Kang, H.; Yun, J.; Lee, J.; Park, J. H.; Baik, S. *ACS Nano* **2011**, *5*, 5088−5093.
(20) Guldin, S.; Huttner, S.; Kolle, M.; Welland, M. E.; Muller-Buschbaum, P.; Friend, R. H.; Steiner, U.; Tetreault, N. *Nano Lett.* **2010**, *10*, 2303−2309.
(21) Ghosh, R.; Brennaman, M. K.; Uher, T.; Ok, M. R.; Samulski, E. T.; McNeil, L. E.; Meyer, T. J.; Lopez, R. *ACS. Appl. Mater. Interfaces* **2011**, *3*, 3929−3935.
(22) Ko, S. H.; Lee, D.; Kang, H. W.; Nam, K. H.; Yeo, J. Y.; Hong, S. J.; Grigoropoulos, C. P.; Sung, H. J. *Nano Lett.* **2011**, *11*, 666−671.
(23) Sauvage, F.; Di Fonzo, F.; Bassi, A. L.; Casari, C. S.; Russo, V.; Divitini, G.; Ducati, C.; Bottani, C. E.; Comte, P.; Grätzel, M. *Nano Lett.* **2010**, *10*, 2562−2567.
(24) Zhang, Q. H.; Gao, L.; Guo, J. K. *Nanostruct. Mater.* **1999**, *11*, 1293−1300.
(25) Chen, R. F.; Zhang, L.; Wei, Y.; Hou, D. L. *J. Mater. Sci.* **2007**, *42*, 7141−7146.
(26) All *d*-spacings were compared with those of bulk value for rutile TiO_2 in JCPDS-ICDD.
(27) Yin, H. B.; Wada, Y.; Kitamura, T.; Sumida, T.; Hasegawa, Y.; Yanagida, S. *J. Mater. Chem.* **2002**, *12*, 378−383.
(28) Sun, J.; Gao, L. *J. Am. Ceram. Soc.* **2002**, *85*, 2382−2384.
(29) Cheng, H. M.; Ma, J. M.; Zhao, Z. G.; Qi, L. M. *Chem. Mater.* **1995**, *7*, 663−671.
(30) Wang, H. L.; He, J. J.; Boschloo, G.; Lindstrom, H.; Hagfeldt, A.; Lindquist, S. E. *J. Phys. Chem. B* **2001**, *105*, 2529−2533.
(31) Weidmann, J.; Dittrich, T.; Konstantinova, E.; Lauermann, I.; Uhlendorf, I.; Koch, F. *Sol. Energy Mater. Sol. Cells* **1999**, *56*, 153−165.
(32) Wu, W. Y.; Shih, T. W.; Chen, P.; Ting, J. M.; Chen, J. M. *J. Electrochem. Soc.* **2011**, *158*, K101−K106.
(33) Wang, Z. S.; Kawauchi, H.; Kashima, T.; Arakawa, H. *Coord. Chem. Rev.* **2004**, *248*, 1381−1389.
(34) Nakade, S.; Kanzaki, T.; Wada, Y.; Yanagida, S. *Langmuir* **2005**, *21*, 10803−10807.

(35) Wang, M.; Chen, P.; Humphry-Baker, R.; Zakeeruddin, S. M.; Grätzel, M. *Chemphyschem* **2009**, *10*, 290−299.
(36) Wang, Q.; Moser, J. E.; Grätzel, M. *J. Phys. Chem. B* **2005**, *109*, 14945−14953.